Received: 28 June 2017 | Revised: 23 November 2017 | Accepted: 25 November 2017

DOI: 10.1111/ffe.12761

ORIGINAL CONTRIBUTION

WILEY

High-temperature testing in a Charpy impact pendulum using in-situ Joule heating of the specimen

P.A. Ferreirós[1,2,3] | P.R. Alonso[1,2] | P.H. Gargano[1,2] | G.H. Rubiolo[1,2,4]

[1]Gerencia Materiales, Comisión Nacional de Energía Atómica (CNEA), Av. Gral. Paz 1499, B1650KNA San Martín, Buenos Aires, Argentina

[2]Instituto de Tecnología J. Sabato, CNEA-UNSAM, Av. Gral. Paz 1499, B1650KNA San Martín, Buenos Aires, Argentina

[3]Universidad Tecnológica Nacional, Facultad Regional General Pacheco (UTN-FRGP), Av. Hipólito Yrigoyen 288, B1617FRP Gral. Pacheco, Buenos Aires, Argentina

[4]Consejo Nacional de Investigaciones Científicas y Técnicas (CONICET), Godoy Cruz 2290, C1425FQB Buenos Aires, Argentina

Correspondence
GH Rubiolo, Gerencia Materiales, Comisión Nacional de Energía Atómica (CNEA), Av. Gral. Paz 1499, B1650KNA San Martín, Buenos Aires, Argentina.
Email: rubiolo@cnea.gov.ar

Abstract

In this paper, an innovative approach to high-temperature testing of subsize Charpy V notched specimens is introduced. The design concept is to heat the specimen on the specimen piece supports up to the moment of impact by flowing AC electric current through it. This approach allows a very accurate centring of the specimen with respect to the anvils and the control of their temperature up to the moment of impact. The temperature profile measured by using the in-situ heating device on ferritic steel specimen over the notch temperature range of 400°C < T < 750°C is presented. The impact energy was measured at different temperatures going through the eutectoid phase transformation of the ferritic steel specimens, with different carbon composition, to investigate the validity of the instrumented in-situ heating method. The method is particularly appropriate to estimate the ductile brittle transition that occurs at high temperature in some metallic alloy systems. Also, its wide range of specimen heating rate provides new research tools for studying, for example, the intermediate temperature embrittlement of metals and alloys.

KEYWORDS

Charpy V-test, ductile-brittle transition, high-temperature tests, impact testing, subsize fracture specimen

1 | INTRODUCTION

The toughness of a material is its ability to absorb energy in the form of plastic deformation without fracturing. In simple terms, it may be defined as the area under the stress-strain curve so it is a parameter that combines both strength and ductility. It should be noted that the stress-strain relationship is dependent on temperature and strain rate so that the toughness will be too.[1]

The toughness of ferritic steels undergoes a transition as the temperature is decreased below the room temperature. At low temperatures, fracture occurs by completely brittle cleavage mechanisms with low levels of absorbed energy. At high temperatures, fracture occurs by ductile dimple mechanisms with absorption of considerable energy. In the transition region, fracture is of a mixed mode. A variety of tests have been used to characterize the ductile-to-brittle transition behaviour in steels. In

Nomenclature: a, = specimen height (y direction); A, = area in the cross section of the specimen (yz plane); A_{C1}, = eutectoid temperature; A_{C3}, = austenitizing temperature; b, = specimen width (z direction); C, = specific heat; D, = density; h, = surface conductance; I, = electric current; P, = perlite phase; s, = perimeter of the cross section of the specimen (yz plane); t, = time; T, = cross-section temperature; T_c, = temperature at the control thermocouple; T_e, = environmental temperature; T_{notch}, = temperature at the notch cross section; α, = ferrite phase; δ, = skin depth; ϵ_m, = strain at maximum force in a tension test at low strain rates; γ, = austenite phase; λ, = thermal conductivity; μ_0, = free space permeability; μ_r, = relative permeability; ρ, = electrical resistivity; ω, = angular frequency of the electric current

addition to differences in specimen size and geometry of the notch (flaw size, shape, and acuity), these techniques strongly differ in the strain rate, and correspondingly, a variety of definitions of transition temperature have emerged. The wide range of testing techniques includes tensile tests,[2] Charpy V-notch impact testing,[3,4] Pellini drop-weight tests,[5,6] impact tensile test,[7] and fracture toughness testing using compact tension and single-edge notched bend specimens.[8,9] In recent years, small punch testing[10,11] was also included in the list. However, the Charpy impact test is undoubtedly the test most commonly used to characterize the ductile-to-brittle transition in steel, and so, the pendulum impact tester is among the first instruments considered to outfit a materials science lab. The characterization of the transition temperature in ferritic steels with Charpy test requires that the temperature of the sample goes from cryogenic to intermediate (~200°C) temperatures.[12] Commonly used temperature conditioning media within the testing community include hot air, hot nitrogen gas, oil bath or water bath to heat, and an alcohol/dry ice bath or cold nitrogen gas to cool the test specimens. American Society for Testing and Materials (ASTM) Standard E23-07[13] specifies a minimum soak time of 5 minutes if the thermal conditioning medium is a liquid and 30 minutes if the medium is a gas. Chosen whatever method for heating or cooling the specimen, the impact of the specimen must occur within 5 seconds after removal from the medium to satisfy the request from E23. The standard does not, however, provide guidance regarding choice of conditioning media and transfer methods, only mentions that the 3 methods used in the past are liquid bath thermal conditioning and transfer to the specimen supports with centring tongs, furnace thermal conditioning and robotic transfer to the specimen supports, and placement of the specimen on the supports followed by in situ heating and cooling. The latter method deserves some level of detail because it heats the specimen on the supports of the Charpy test machine as our development but differs in the thermal conditioning principle and operating range of temperatures. The method, covered by US Patent Number 5,770,791,[14,15] claim that standard or subsized Charpy V-notch specimens can be heating or cooling on the test machine itself over the temperature range of $-180°C < T < 315°C$ by flowing a thermally conditioned gas over the surfaces of the specimen, which contain the volume of material near the notch.

Beyond the ferritic steels, the ductile brittle transition occurs at high temperature in other metallic alloy systems such as gamma titanium aluminide alloys,[16] tungsten alloys,[17,18] WC-Co alloys,[19] Mo-Si-B alloys,[20] Fe-Al alloys,[21,22] and NiAl-based alloys.[23] Little use has been made of impact toughness testing at elevated temperatures of these alloy systems owing to the great scatter of the results linked to the difficulties involved in creating identical temperature conditions for tests on a large number of specimens. The time required for transferring the specimen from the furnace to the supports of the impact testing machine is different in each individual case. Consequently, the temperature of the specimen at the moment of impact is also different in each individual case,[24] even if a thermocouple attached to the sample surface is used because the internal temperature of the sample differs considerably with respect to the surface temperature.[25] When subsize Charpy V-notch specimens are tested, the heat losses over the time interval to transfer the specimen to the pendulum impact are even greater. To overcome this, we propose to heat the specimen on the specimen support up to the moment of impact by using the Joule effect and this approach is the subject of this paper.

2 | DEVICE FOR HIGH-TEMPERATURE IMPACT TESTS IN A CHARPY MACHINE

The design concept is to heat the specimen on the specimen piece supports up to the moment of impact by flowing AC electric current through it. The designed device for Charpy tests at high temperatures with in-situ heating is presented schematically in Figure 1A. The device has 2 pneumatically operated arms that clamp the specimen against the specimen piece supports of the testing machine. At the end of the arms, electrically isolated, copper terminals are connected to the electrical circuit. The terminals press the ends of the specimen and are refrigerated by a water cooling circuit. The anvils and specimen piece supports of the testing machine are painted with epoxy paint to achieve electrical isolation from the specimen. The electrical circuit for heating consists of a high current-low voltage transformer whose input AC voltage is handled by a temperature controller led by a thermocouple welded to the specimen.

The operational system diagram (heating electrical circuit and clamping device) is shown in Figure 1B. The specimen with the attached control thermocouple (T_c) is placed on the piece supports and clamped when the pneumatic solenoid valve is manually actuated. The test temperature is selected in the temperature controller. The controller supplies the electrical power to the transformer and an AC current (i) is applied on the specimen. Once the test temperature is reached and stabilized, the pendulum fall is manually actuated. An optical sensor located in the path of the pendulum interrupts the electric current and acts on the pneumatic solenoid valve

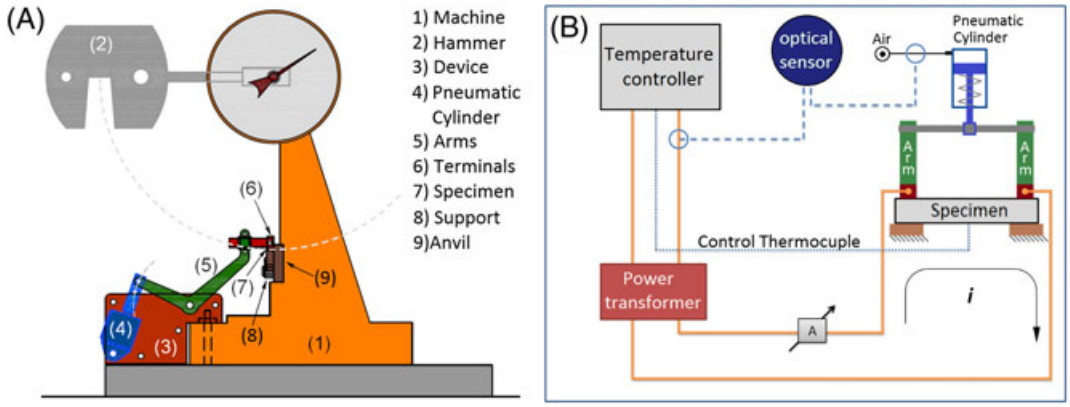

FIGURE 1 Scheme of equipment for high temperature Charpy test. A, Machine and device. B, Operational system diagram [Colour figure can be viewed at wileyonlinelibrary.com]

releasing the clamp and separating the copper terminals from the sample. Finally, the impact of the pendulum against simply supported specimen occurs. The position of the optical sensor sets the time elapsed because the electrical power is stopped till the striker hits the specimen.

Because of the chosen heating method, a symmetric temperature gradient around the position of the notch in the specimen is expected. So, a key element of the approach is to ensure that the fracture process volume is thermally conditioned. Plane strain 3-dimensional finite element analyses of the plastic zone in a Charpy specimen as a function of applied load by Manahan et al26 show that the plastic zone extent tends to peak at about 1 specimen height. Therefore, the fracture process zone extends along the axis of the specimen by 1 specimen height on both sides of the crack plane. This volume of material must be kept at the desired test temperature up to the time when the striker contacts the specimen.

3 | EXPERIMENTAL PROCEDURES

This section presents the instrumentation of a commercial Charpy impact test machine with the innovative device designed for high-temperature impact tests and the materials used to completely validate the in-situ high-temperature heating technology.

Figure 2 shows the new device instrumented on a pendulum Charpy impact machine Otto Wolpert-Werke PW 5 S5 having a capacity of 50 J (minimum division of 0.5 J) and an impact velocity of 3.8 m s^{-1}. The picture also shows the AC transformer (output: 4 V - 1000 A maximum).

The materials tested were AISI 1010, 1045, and 1080 carbon steels in the annealed condition. The content of C and S of steel was measured on a Leco CS200 analyser (see Table 1). Microstructural observations were made in a Philips Quanta 200 Scanning Electron Microscope (SEM). Rockwell hardness was measured in a NRZ testing machine by using a 100 kgf load and 1/16″ spherical diameter indenter.

V-notch Charpy impact specimens were machined from 4.76-mm-thick sheets. Specimen dimensions (2.5 × 10 × 55 mm) and notch geometry were in accordance with the subsize specimen ASTM E23-07 recommendations.[13] The orientation of the specimens tested is longitudinal-transverse (*LT*). The thickness of paint on the anvils and the sample is about 50 μm, which is less than the tolerance in the geometric dimensions of ASTM E23-07 test specimens.[13] However, several AISI 1045 steel specimens were used to evaluate deviations in the Charpy impact energy coming from the paint as well as from the specimen clamping system. Two types of experiments were performed at room temperature, 1 with painting and clamping while the other was free of them. The difference in the average absorbed energy of 5 determinations for each type of experiment is less than their respective standard deviations; therefore, there is no detectable deviation in the absorbed energy because of the proposed in-situ heating device.

An AISI 1045 steel specimen was used for the measurement of the temperature gradient at different values of the control thermocouple in the range of 400°C to 700°C. Thermocouple type K (chromel/alumel) of 0.1-mm wire diameter were arc-welded along the x direction, see dashed line in Figure 3. The control thermocouple was located at $x = 3$ mm from the notch. A NOVUS Field Data Logger with an acquisition frequency of 0.5 seconds was used for simultaneous recording of the thermocouple output values. Meanwhile, thermographic measurements were taken with a FLIR T640 infrared thermal imaging camera and the electrical current through the Charpy specimen was measured with a clamp metre.

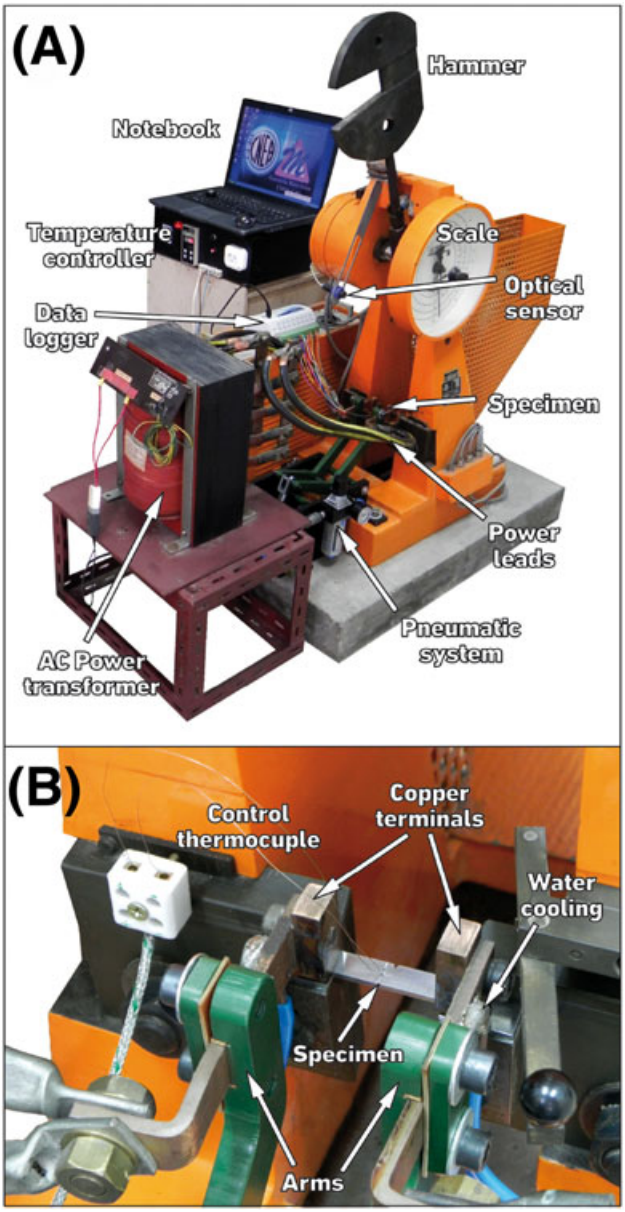

FIGURE 2 A, Photograph of Charpy machine with the high temperature device. B, Details of the electrical terminals and the clamping system [Colour figure can be viewed at wileyonlinelibrary.com]

TABLE 1 Carbon and sulfur contents and hardness of steels

Carbon Steel	C (wt%)	S (wt%)	HR_B
AISI 1010	0.11 ± 0.01	0.0093 ± 0.0009	70
AISI 1045	0.47 ± 0.03	0.037 ± 0.004	89
AISI 1080	0.78 ± 0.06	0.0061 ± 0.0006	98

The Charpy tests were carried out from room temperature up to 800°C. Only 1 sample was tested at each temperature and alloy composition.

The information obtained from the impact tests was the absorbed energy and the lateral contraction in function of the temperature. The lateral contraction was chosen instead of the lateral expansion (as recommended by ASTM E23-07) because of the geometry of our subsize specimen. This specimen has the ligament behind the notch larger than the thickness so that the slip for plastic deformation develops through the thickness on planes at approximately 45°. This through-thickness mode of slip should suppress the bend mode characteristic of the full-size Charpy specimen losing sensitivity when measuring lateral expansion.[27,28] The methodology to measure the lateral contraction capture a digital image (at 5X magnification) of the fracture surface and measure the length between fracture sides, in thickness direction ahead of notch, using an image analysis software. The digital image was taken with an Olympus BX60M microscope equipped with an Olympus U-TV0.5XC-3 camera. The error involved in this measurement is 0.01 μm. The minimum length between fracture sides of the fracture surface of both halves of the specimen was measured. The lateral contraction was calculated as the average of both measurements, and its error was estimated as half of the difference.

4 | RESULTS AND DISCUSSION

4.1 | Thermal studies on the specimen heating in-situ

Measurements using the specimen instrumented with thermocouples are shown in Figure 4. Each data set was measured at a specified control temperature. The indicated temperatures were calculated by averaging the values in stable control periods of 120 seconds; their standard deviations were lower than 4°C. The specimen is clamped with the refrigerated electrical contacts (x = 19.25 mm); therefore, the temperature in its ends is constant and independent of test temperature. The temperature profiles in Figure 4 indicate a longitudinal thermal gradient to notch of around $(0.01 * T_{notch})^{\circ}$C/mm.

In addition to the thermocouple measurements in the x direction of the sample, the 3 thermal images of Figure 5 allow us to estimate the temperature profiles along the y direction of the specimen. Figure 5E shows these temperature profiles for 2 x positions (in the notch ($x = 0$) and in the control thermocouple ($x = 3$ mm)) and three different control temperatures. At the x position of the notch and for T_c = 700°C, it can be measured a mild thermal gradient of 2.5°C/mm along the y direction.

Figure 6 shows the evolution of temperature versus time as registered by the thermocouple placed at the crack plane just below the notch ($x = 0$) during several heating-cooling cycles for T_c in the range of 400°C to 700°C. The heating ramps are approximately linear with a rate of 32°C/s and independent of the maximum temperature at

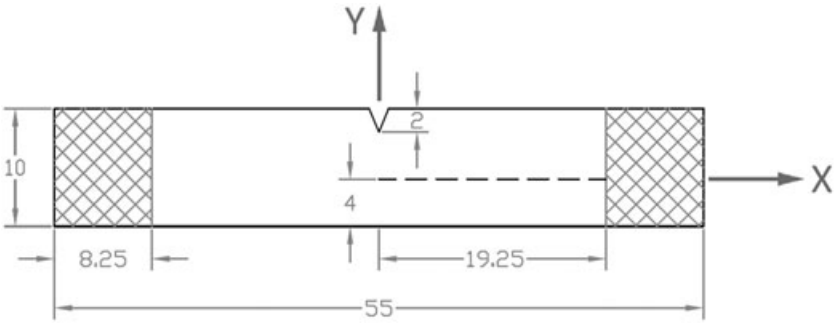

FIGURE 3 Sample drawing with dimensions in mm and the reference system adopted. The gridding indicates the electrical contact zones, and the dotted line indicates the thermocouples welding sites

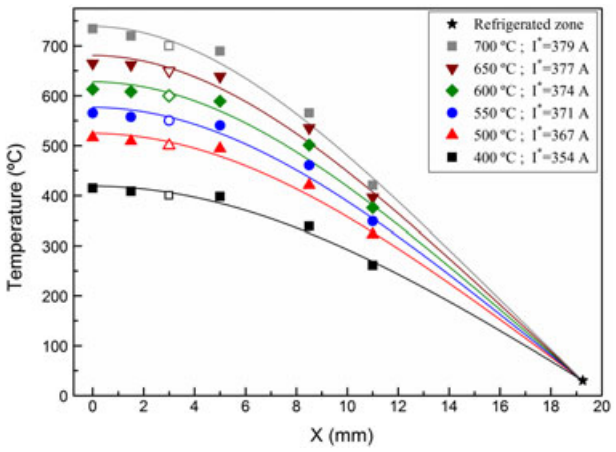

FIGURE 4 Temperature profiles of an AISI 1045 (2.5 × 10 × 55 mm) V-notch Charpy impact specimen heated by AC current. The symbols are measured values, and the solid lines are results from numerical solution of the thermal model implemented in Equation A1. The open symbols represent the control thermocouple value (T_c) [Colour figure can be viewed at wileyonlinelibrary.com]

the notch. They are followed by an isothermal stability step and ends with the cooling step at 0 electrical current. As expected, the magnitude of the cooling rate is dependent on the maximum temperature reached in the notch. The larger the maximum temperature reached in the notch, the larger the cooling rate. As an example, we measured an initial drop of 100°C in times of 4 and 11 seconds for $T_{\text{notch}} = 734°C$ ($T_c = 700°C$) and $T_{\text{notch}} = 412°C$ ($T_c = 400°C$), respectively. Because the elapsed time from the interruption of electrical power to the impact is 0.1 second, the temperature drop at the impact time is less than 2.5°C for the tested temperature range. These temperature drops are less than the thermal oscillation produced by the temperature control system; thus, the current in-situ heating device meets the requirement that the temperature of the specimen at the time of impact is known.

Our measurements show that there is significant variation of the temperature within the fracture process volume but the extent of this could be related with the control temperature. If so, the mean value and the confidence interval of the temperature in the fracture process volume could be reported with accuracy from the value of the control temperature. To test this hypothesis in a quantitative manner, we have implemented a thermal model based on heat flow theory to know the temperature distribution function of the specimen that fits the experimental data obtained along the specimen through the thermocouples (see Appendix A). The calculated temperature profiles are included as solid curves in Figure 4. Having the calculated temperature profile of the specimen, we obtained a graph of the temperature at the notch and at the boundary of the fracture process volume (2.5 mm from the crack plane) versus the control temperature as shown in Figure 7. The linear dependence between these variables is an unexpected but technologically important result because it enables a simple formula for evaluating the mean value and the confidence interval for the temperature in the fracture volume from the value of the control temperature. Mainly, this thermal study demonstrates that in-situ heating of Charpy specimen by AC current produces a temperature gradient in the fracture process volume whose limits can be known by calculation or by direct measurement. Prior knowledge of these limits qualifies this procedure in the Charpy test for evaluating the ductile-brittle transition at high temperatures of a particular material.

4.2 | Charpy tests at high temperature

The plastic-flow behaviour of ferrite + pearlite mixtures in carbon steels has received most attention in the past.[29,30] Flow stress and strain at maximum force (ϵ_m) as function of temperature were obtained with tension test at low strain rates. For all carbon content up to the eutectoid composition (0.77 wt% C), the overall behaviour of the flow stress and ϵ_m is to decrease with temperature displaying a discontinuity located around the eutectoid phase transformation temperature. In the case of ϵ_m, the discontinuity is a sharp increment whose intensity enhances with the perlite volume. On the other hand, the behaviour of the discontinuity in the flow stress is more complicated. Because the strength of the austenite

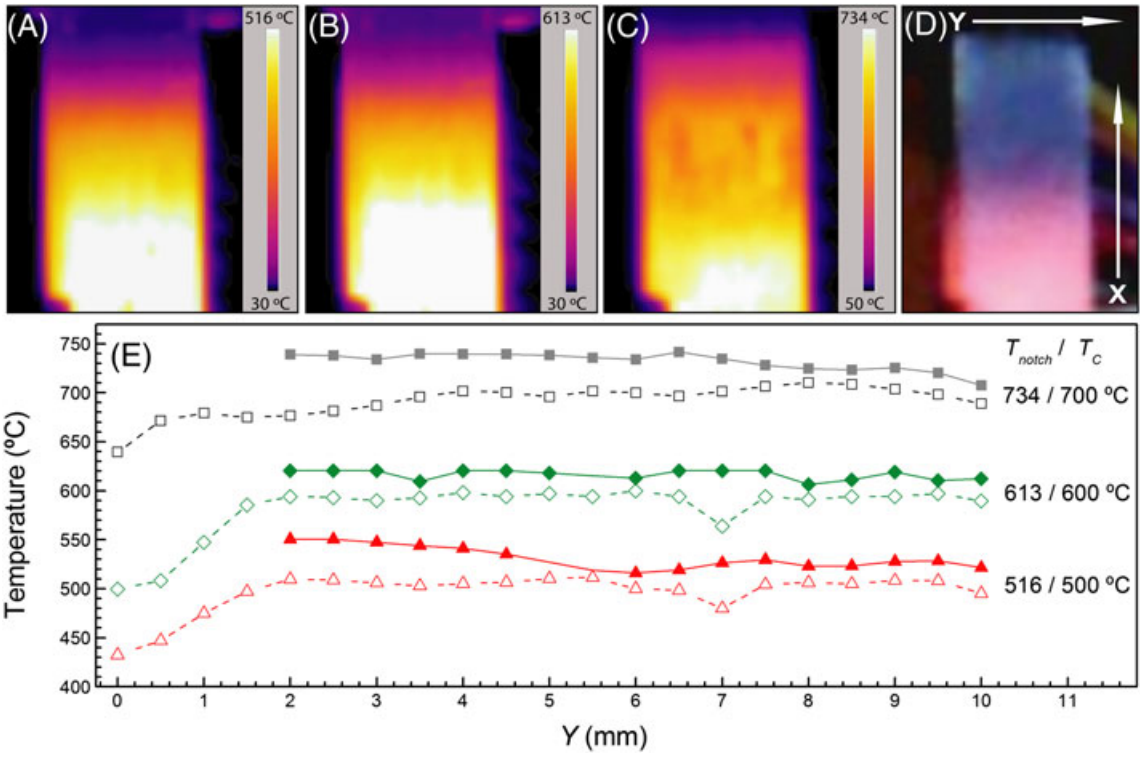

FIGURE 5 Thermographs of the specimen during the measurement of the temperature profiles of Figure 4: A, $T_c = 500°C$; B, $T_c = 600°C$; and C, $T_c = 700°C$. D, Photograph of the specimen at $T_c = 700°C$. E, Temperature profiles measured from the thermographs (fill symbol for T_{notch} and open symbol for T_c) [Colour figure can be viewed at wileyonlinelibrary.com]

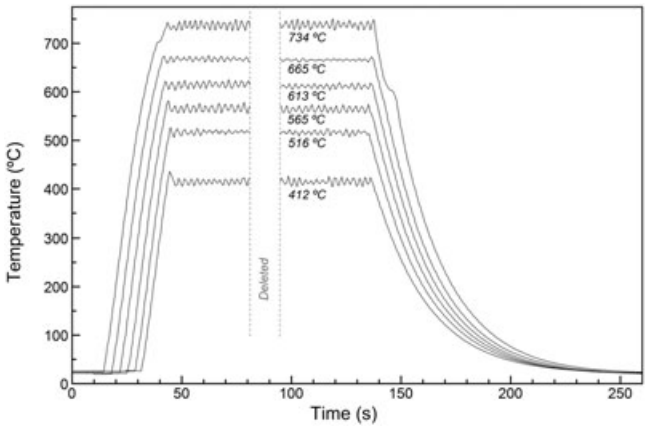

FIGURE 6 Thermal cycles registered by the thermocouple placed at the crack plane just below the notch ($x = 0$)

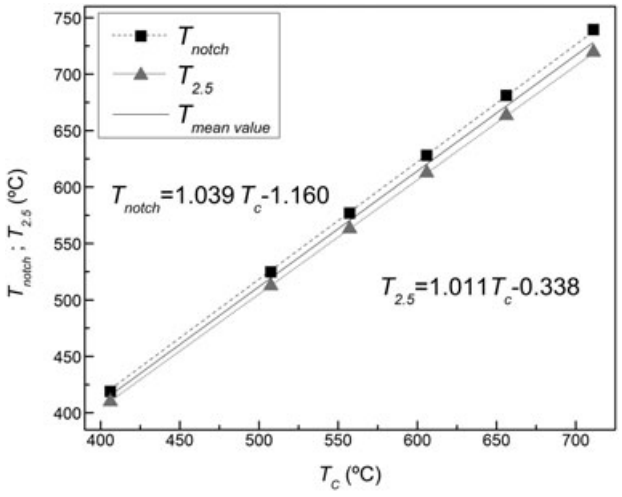

FIGURE 7 Confidence interval for the temperature at the fracture process volume as function of the control temperature

phase is higher than that of ferrite phase and less than the pearlite phase, the sharp transition of the flow stress occurring at the eutectoid temperature of a mixture of ferrite + pearlite may increase or decrease the flow stress depending on the pearlite volume. From these results, 1 can guess that the toughness of these steels might show a discontinuity in the same temperature range. So, we propose to study this material property by using our in-situ heating technology for the pendulum Charpy impact machine.

Scanning electron microscope photographs of the tested steel microstructure can be seen in Figure 8. These microstructures are typical of ferrite/pearlite carbon steels in the furnace annealed condition. In this imaging, smooth areas tend to be dark, and carbides standing in relief above etched ferrite are brighter; this is generally opposite to the contrast seen using optical microscopy. So, the softer constituent (ferrite) appears dark gray in

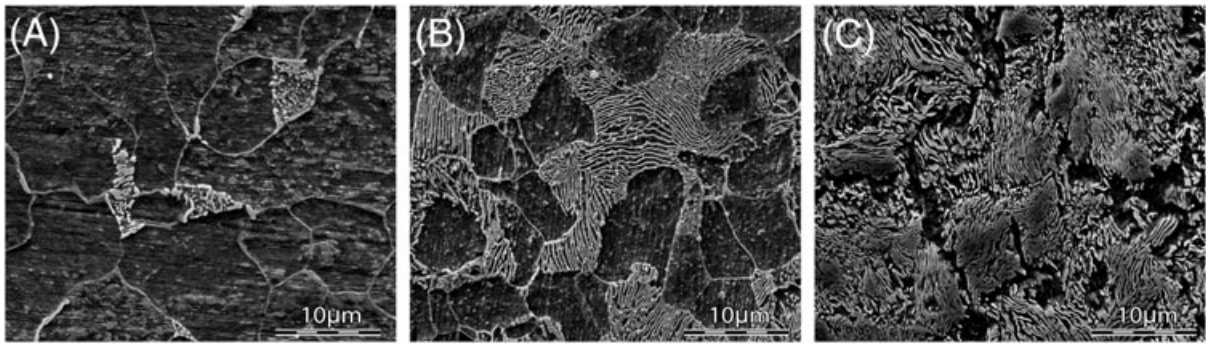

FIGURE 8 Microstructures of tested steels in the furnace annealed condition: A, AISI 1010; B, AISI 1045; and C, AISI 1080

colour while the harder constituent (lamellar pearlite) looks light gray. The thickness of the ferrite network across the pearlite colonies decreases as the carbon content increases.

To preserve the initial lamellar perlite microstructure for test temperatures below the eutectoid transformation, the heating cycle for all Charpy test comprises an initial stage with a heating rate of about 32°C/s, as shown in Figure 6, followed by a hold time of 6 seconds before the hammer contact the specimen. This short heating cycle is only possible because of the chosen heating method.

The variation in Charpy impact energy and lateral contraction with temperature of tested ferrite/pearlite carbon steels from room temperature up to about 800°C is presented in Figures 9 and 10, respectively (note that only 1 specimen was tested per alloy at a given temperature). The error bars show the confidence interval for the temperature in the fracture volume as estimated by the method of Figure 7. In contrast, the error bars for

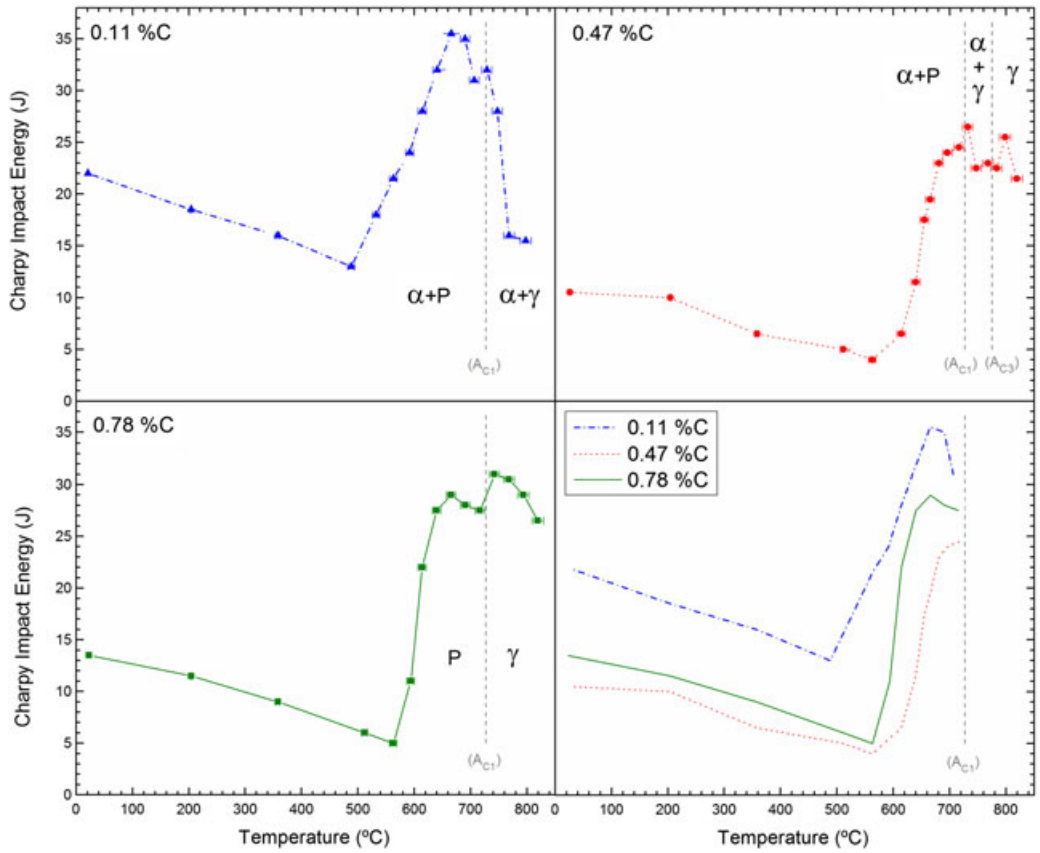

FIGURE 9 Variation of Charpy impact toughness with test temperature for several ferrite/pearlite carbon steels. The eutectoid temperature (A_{C1}) and the austenitizing temperature (A_{C3}) are shown as a vertical dashed line.[31] The letters α, P, and γ are used to denote the phases ferrite, perlite, and austenite, respectively [Colour figure can be viewed at wileyonlinelibrary.com]

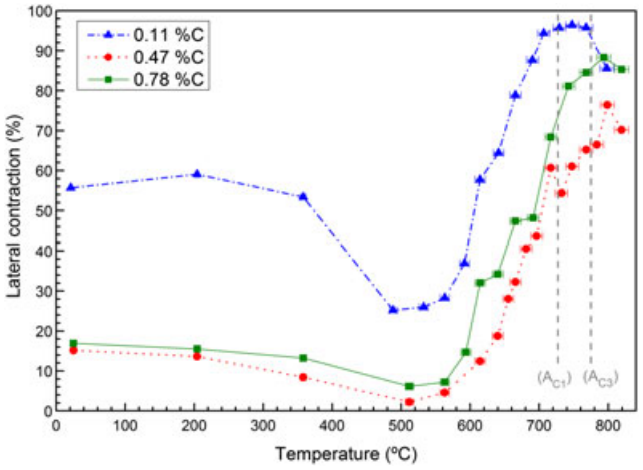

FIGURE 10 Variation of the lateral contraction with test temperature of Charpy V-notched specimens for several ferrite/pearlite carbon steels. The eutectoid temperature (A_{C1}) and the austenitizing temperature for the 0.47%C steel (A_{C3}) are shown as a vertical dashed lines [Colour figure can be viewed at wileyonlinelibrary.com]

impact energy and lateral contraction were not added in the figures because these were very small (for example, the largest measurement error found in lateral contraction was ±0.84% of the sample thickness).

For all carbon content, the impact toughness decreases slowly from room temperature up to around 500°C and, at the same temperature, increased volume fraction of pearlite lower the toughness. A steep toughness jump appears at around 500°C and ends at the eutectoid temperature; the amount of perlite increases starting temperature of this jump but the height of the jump is independent. The lateral contraction, the parameter correlating with plastic deformation in the Charpy-V test, resembles that behaviour. These last findings are new in the literature but they are in agreement with the softening behaviour observed in tensile[30,32] and hot-microhardness[33] test of ferrite/pearlite carbon steels. The observed thermal softening of pearlitic steels can be related to the increase in deformability of cementite with temperature as revealed by Inoue et al.[34] In that study, they evaluated the effect of temperature on the deformation and fracture of cementite in steels. Their findings indicate that cementite becomes highly deformable for temperatures above 400°C. As a consequence, for temperatures above 400°C, the deformation of pearlite is no longer exclusively controlled by the movement of dislocations within the ferrite, but also in the cementite layers leading to an overall softer response.

Figure 11 shows a SEM view of the fracture surface of all steels cracked by impact at room temperature. In all cases, the fracture surface is characterized by a honeycomb structure with 2 regions of different cell size. The larger cell size region shows a dimple fracture mechanism, which is typical for high-ductility metals, and which is formed by microvoid initiation, microvoid coalescence, and microvoid-induced crack propagation under tensile loading. Dimples are formed when the walls of the voids break upon contraction. Most of the time, nonmetallic inclusions (ie, sulphides/oxides) are found at the bottom of these dimples as those signposted by small (yellow) arrows in Figures 11A and 11B. Instead of this, the walls of the honeycomb with the smaller cell size show cleavage facets (see details in Figures 12A and 12C) because of a brittle fracture as also occurs with the nonmetallic inclusions inside them (see the inclusion signposted by the large [red] arrow in Figure 11B). The size of the regions with cleavage facets corresponds, as a rule, to the size of pearlite colonies, and therefore, the honeycomb walls in those regions are identified as cementite plates. Whereas the region with the dimple fracture surface is identified as the ferrite matrix. According to the model suggested

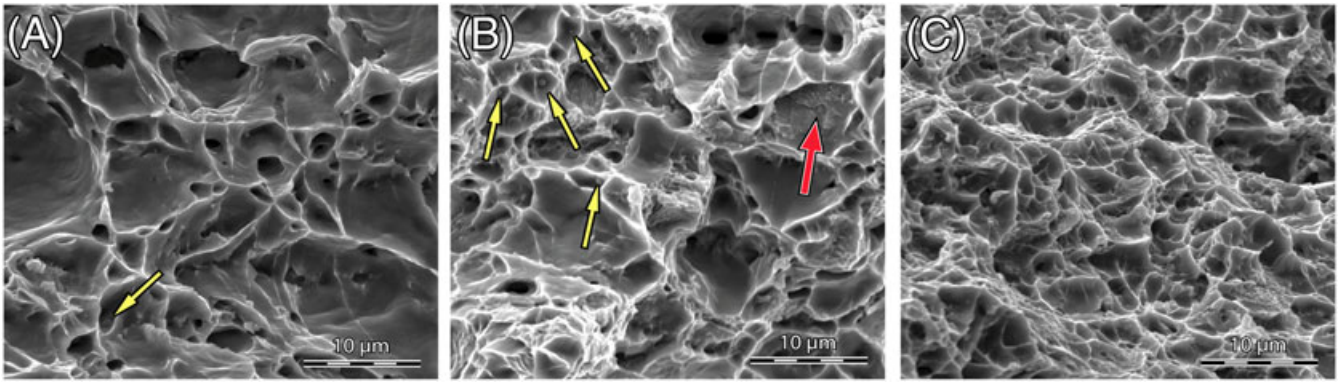

FIGURE 11 Scanning electron microscope (SEM) fractographs showing details of the fracture surface of the steels cracked by impact at room temperature. A, AISI 1010; B, AISI 1045; and C, AISI 1080. The small (yellow) arrows indicate the inclusions in the bottom of the microvoids in the ferritic matrix of the steel. The large (red) arrow indicates the cleavage fracture of an inclusion inside a pearlite colony [Colour figure can be viewed at wileyonlinelibrary.com]

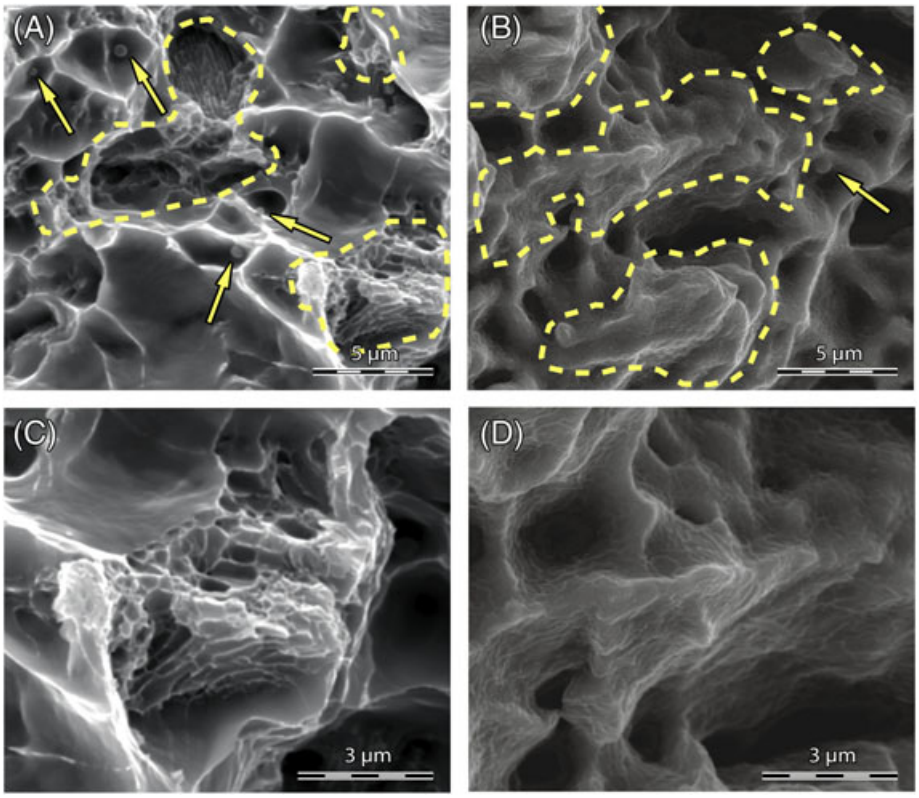

FIGURE 12 Scanning electron microscope (SEM) fractographs showing details of the fracture in the pearlite colonies of the AISI 1045 steel cracked by impact at room temperature (A and C) and at 640°C (B and D) [Colour figure can be viewed at wileyonlinelibrary.com]

by Miller and Smith,[35] the microvoid in lamellar pearlite can also nucleate as a result of cracking of cementite plates under the action of external loading. All of these features together with the mechanical properties reported above suggest that at temperatures lower than 500°C, the crack nucleates within pearlite colonies and develop slowly inside the ductile ferrite up to the collapse.

The effect of a test temperature greater than 500°C on the impact rupture mechanism can be seen in the SEM fractography of Figures 12B and 12D; the cementite plates show now the same break upon contraction as the walls of the voids in the ferrite. This observation agrees with the proposed softening mechanism to explain the increase in toughness at temperatures above 500°C and up to the eutectoid transformation temperature.

The effect of the eutectoid transformation (A_{C1}) on the impact toughness is well defined in the results of the almost fully pearlitic sample with 0.78%C (Figure 9). There is an abrupt rise of toughness because of the higher ductility of the austenitic phase, which replaces, through the eutectoid transformation, the same volume occupied by the pearlite. The subsequent increase of temperature above the eutectoid reduces austenite toughness in the same way as occurs in the ferrite phase. Because of the high ductility of the samples around the eutectoid transformation temperature, the lateral contraction data are unable to account for such a fine detail. The results of samples with 0.47%C and 0.11%C show that the discontinuity in toughness is reduced as the volume fraction of pearlite is lower in the pearlite + ferrite system. In these cases, the rate of decrease in toughness above the eutectoid temperature is higher than the 0.78%C sample because of the ferrite + austenite mixture instead of almost fully austenite. Once again, these results are new in the literature, but agree with increasing ductility observed in tensile failure of ferrite/pearlite carbon steels at the eutectoid temperature.[31] Because there is indirect experimental information indicating a transition in toughness of the pearlite + ferrite system following the eutectoid transformation of austenite to pearlite and that the temperature of said transformation is a thermophysical property of the system, our results validate the in-situ heating technology to estimate the ductile brittle transition temperature with subsize impact test specimens at elevated temperatures.

5 | CONCLUSIONS

The device developed for the heating of the specimen on the supports of the Charpy testing machine, by flowing AC electric current through it, reduces the uncertainty

associated with thermal losses during transfer of a test specimen from the furnace to the test machine and also improves the alignment of the specimen in the test machine. The results obtained from impact energy tests of subsize specimens using the in-situ method have proved to be sensitive with respect to a well-known phase transformation temperature in ferritic/perlitic steels.

Although the initial impetus for the development of this new technology was to estimate the ductile brittle transition that occurs at high temperature in some metallic alloy systems, we find that its wide range of specimen heating rate provides new research tools for studying, for example, the intermediate temperature embrittlement of metals and alloys that has been an area of intense research since 1912.[36]

ACKNOWLEDGEMENTS

The authors thank Ing. A. F. Iorio (Gerencia Materiales, CNEA) who supplies the Charpy machine wherein the device for high-temperature test was placed. They also thank P. Penas and D. P. Acosta (both from Gerencia Desarrollo, Ensayos y Gestión de Vida, CNEA) for thermographic measurements.

ORCID

G.H. Rubiolo http://orcid.org/0000-0001-5277-775X

REFERENCES

1. Viswanathan R. *Damage mechanisms and life assessment of high-temperature components*. Metals Park, Ohio 44073: ASM International; 1993:21-45.
2. Ritchie RO, Knott JF, Rice JR. On the relationship between critical tensile stress and fracture toughness in mild steel. *J Mech Phys Solids*. 1973;21(6):395-410.
3. Siewert, T. A., Manahan, M. P., McCowan, C. N., Holt, J. M., Marsh, F. J., Ruth, E. A. (2000) The history and importance of impact testing. In: Siewert, T.A., Manahan, M.P. Sr., (Eds.), *Pendulum Impact Testing: A Century of Progress, ASTM STP 1380*, American Society for Testing and Materials, West Conshohocken, PA., 3-16.
4. Sapora A, Firrao D. Finite fracture mechanics predictions on the apparent fracture toughness of as-quenched Charpy V-type AISI 4340 steel specimens. *Fatigue Fract Eng Mater Struct*. 2017;40(6):949-958.
5. Krasowsky AJ, Kashtalyan YA, Krasiko VN. Brittle-to-ductile transition in steels and the critical transition temperature. *Int J Fracture*. 1983;23(4):297-315.
6. Chen L, Yao X, Cen S, Wang S. Normal impact behaviour of C/SiC rigid-felt titanium alloy three layered plate. *Fatigue Fract Eng Mater Struct*. 2016;39:1433-1442.
7. Bayraktar E, Kaplan D, Schmidt F, Paqueton H, Grumbach M. State of art of impact tensile test (ITT): its historical development as a simulated crash test of industrial materials and presentation of new "ductile/brittle" transition diagrams. *J Mater Process Technol*. 2008;204(1-3):313-326.
8. Lei W, Yao M. A new model of the critical crack size for low temperature brittle fracture of structural steel and its experimental verification. *Engng Fract Mech*. 1994;49:225-234.
9. Khor W, Moore PL, Pisarski HG, Haslett M, Brown CJ. Measurement and prediction of CTOD in austenitic stainless steel. *Fatigue Fract Eng Mater Struct*. 2016;39:357-371.
10. Manahan MP, Argon AS, Harling OK. The development of a miniaturized disk bend test for the determination of postirradiation mechanical properties. *J Nucl Mater*. 1981;104:1545-1550.
11. Alegre JM, Cuesta II, Barbachano HL. Determination of the fracture properties of metallic materials using pre-cracked small punch tests. *Fatigue Fract Eng Mater Struct*. 2015;38(1):104-112.
12. American Society for Metals. Vander Voort G. F. Embrittlement of Steels. In: *ASM Handbook*. Vol.1 Materials Park, OH: Properties and Selection: Irons, Steels, and High Performance Alloys, Section: Service Characteristics of Carbon and Low-Alloy Steels; 2005:1058-1133.
13. ASTM Standard E23-07a. *Standard Test Methods for Notched Bar Impact Testing of Metallic Materials*. West Conshohocken, PA: ASTM; 2007:1-28.
14. Manahan MP. Method and apparatus for accurate measurement of impact fracture behavior. *US Patent Number 5*. 1998;770(791):1-23.
15. Manahan MP Sr. In: Siewert TA, Manahan MP Sr, eds. *"In-situ Heating and Cooling of Charpy Test Specimens," Pendulum Impact Testing: A Century of Progress, STP 1380*. West Conshohocken, PA: American Society for Testing and Materials; 2000.
16. Appel F, Paul JDH, Oehring M. *Gamma Titanium Aluminide Alloys: Science and Technology*. Weinheim, Germany: John Wiley & Sons; 2011:125-401.
17. Lang S, Yang Q, Sun N, et al. Microstructure, basic thermal–mechanical and Charpy impact properties of W-0.1 wt.% TiC alloy via chemical method. *J Alloys Compd*. 2016;660:184-192.
18. Tejado E, Carvalho PA, Munoz A, et al. The effects of tantalum addition on the microtexture and mechanical behaviour of tungsten for ITER applications. *J Nucl Mater*. 2015;467:949-955.
19. Milman YV. The effect of structural state and temperature on mechanical properties and deformation mechanisms of WC-Co hard alloy. *J Superhard Mater*. 2014;36(2):65-81.
20. Zhang L, Pan K, Lin J. Fracture toughness and fracture mechanisms in Mo_5SiB_2 at ambient to elevated temperatures. *Intermetallics*. 2013;37:49-54.
21. Krein R, Palm M, Heilmaier M. Characterization of microstructures, mechanical properties, and oxidation behaviour of coherent A2+$L2_1$ Fe–Al–Ti. *J Mater Res*. 2009;24(11):3412-3421.
22. Risanti D, Deges J, Falat L, et al. Dependence of the brittle-to-ductile transition temperature (BDTT) on the Al content of Fe-Al alloys. *Intermetallics*. 2005;13(12):1337-1342.

23. Chen RS, Guo JT, Zhou WL, Zhou JY. Brittle-to-ductile transition of a multiphase intermetallic alloy based on NiAl. *Intermetallics*. 2000;8(5-6):663-667.

24. Kumar KS, Pang L. Effect of temperature and strain rate on the mechanical properties of Fe-40Al-0.6C. *Mater Sci Eng A*. 1998;258(1-2):153-160.

25. Pang L, Kumar KS. On the impact toughness of Fe-40Al-based B2 aluminides. *Intermetallics*. 2000;8(2):157-163.

26. Manahan MP, Stonesifer RB, Soong Y, Burger JM. Miniaturized notch test specimen and test machine design. In: Siewert TA, Schmieder K, eds. *Pendulum Impact Machines: Procedures and Specimens for Verification, ASTM STP 1248*. West Conshohocken, PA: American Society for Testing and Materials; 1995:39-69.

27. Gross JH. Effect of strength and thickness on notch ductility. In: *Impact Testing of Metals, ASTM STP 466*. Philadelphia, PA: American Society for Testing and Materials; 1970:21-52.

28. Shoemaker AK. Notch-ductility transition of structural steels of various yield strengths. *Trans ASME J Engng Ind*. 1972;94(1):299-306.

29. Wray PJ. High temperature plastic-flow behavior of mixtures of austenite, cementite, ferrite, and pearlite in plain-carbon steels. *Metall Trans A*. 1984;15(11):2041-2058.

30. Wray PJ. Tensile failure behavior of plain carbon steels at elevated temperatures. *Metall Trans A*. 1984;15(11):2059-2073.

31. Okamoto H. The C-Fe (carbon-iron) system. *J Phase Equilib*. 1992;13(5):543-565.

32. Pina JC, Kouznetsova VG, Geers MGD. Elevated temperature creep of pearlitic steels: an experimental-numerical approach. *Mech Time-Depend Mater*. 2014;18(3):611-631.

33. Torres H, Varga M, Rodríguez Ripoll M. High temperature hardness of steels and iron-based alloys. *Mater Sci Eng A*. 2016;671:170-181.

34. Inoue A, Ogura T, Masumoto T. Microstructures of deformation and fracture of cementite in pearlitic carbon steels strained at various temperatures. *Metall Trans A*. 1977;8(11):1689-1695.

35. Miller LT, Smith GS. Tensile fracture in carbon steels. *J Iron Steel Inst*. 1970;208:988-1005.

36. Zheng L, Schmitz G, Meng Y, Chellali R, Schlesiger R. Mechanism of intermediate temperature embrittlement of Ni and Ni-based superalloys. *Crit Rev Solid State Mater Sci*. 2012;37(3):181-214.

37. Carslaw HS, Jaeger JC. *Conduction of heat in solids*. Oxford: Oxford University Press; 1959:133-187.

38. Rubiolo, GH, Petersen, C. Axial temperature distribution of an ohmic heat H-GRIM specimen under stationary conditions. Karlsruhe Nuclear Research Center, Report 03-02-02P59A, 1988; 1-11.

39. American Society for Metals. Physical properties of carbon and low-alloy steels. In: *ASM Handbook*. Vol.1 Materials Park, OH: Properties and Selection: Irons, Steels, and High Performance Alloys, Section: Carbon and Low-Alloy Steels; 2005:330-333.

40. Landau LD, Lifshitz EM, Pitaevskii LP. *Electrodynamics of Continuous Media*. Secon ed. Oxford: Pergamon Press; 1984:208-210.

41. Morishita M, Takahashi N, Miyagi D, Nakano M. Examination of magnetic properties of several magnetic materials at high temperature. *Przegląd Elektrotechniczny*. 2011;9b:106-110.

How to cite this article: Ferreirós PA, Alonso PR, Gargano PH, Rubiolo GH. High-temperature testing in a Charpy impact pendulum using in-situ Joule heating of the specimen. *Fatigue Fract Eng Mater Struct*. 2017;1-12. https://doi.org/10.1111/ffe.12761

APPENDIX A.

AXIAL TEMPERATURE DISTRIBUTION OF A V-NOTCH CHARPY IMPACT SPECIMEN HEATED USING THE JOULE EFFECT

The thermal model assumed that the cross sections of the specimen have a constant temperature, but its area (A) and perimeter (s) vary in the axial direction because of the notch.[37] The heat flux is taken unidirectional along the x axis of the specimen. The heat source comes from the Joule effect produced by the electric current (I), and the heat loss occurs by conduction to the ends of the specimen and by radiation from the surface of the specimen to the environment. So, the total rate of heat gain in a volume element of the specimen is

$$A\,D\,C\,\frac{\partial T}{\partial t}=\frac{\partial}{\partial x}\left(\lambda\,A\,\frac{\partial T}{\partial x}\right)-h\,s\,(T-T_e)+\frac{I^2\rho}{A} \qquad \text{(A1)}$$

where T is the specimen temperature at x position, T_e is the environmental temperature, C is the specific heat, D is the density, ρ is the electrical resistivity, h is the surface conductance, and λ is the thermal conductivity. Our interest is the case of steady temperature in which T does not vary with the time and Equation A1 becomes equal to 0. Then, the differential equation was numerically solved for $T_{(x)}$ through a finite differences method with the boundary conditions $\partial T/\partial x_{(x\,=\,0)}=0$ and $T_{(x\,=\,19.25\ \mathrm{mm})}=30^{\circ}\mathrm{C}$.[38] The electrical resistivity and the thermal conductivity were expressed as linear functions of the temperature fitted to literature data for AISI 1042 steel.[39] A surface conductance of 7.5 $W/^{\circ}\mathrm{C\ m^2}$ was used for all temperatures. For each control temperature, the difference between modelled and experimental temperature profiles $T_{(x)}$ was minimized through a least squares method where the fitting output value was the electrical current (I^*). The calculated temperature profiles are included as solid curves in the Figure 4 of the main text. We found different values for measured (I) and modelled (I^*) electric currents as can be seen in Figure A1.

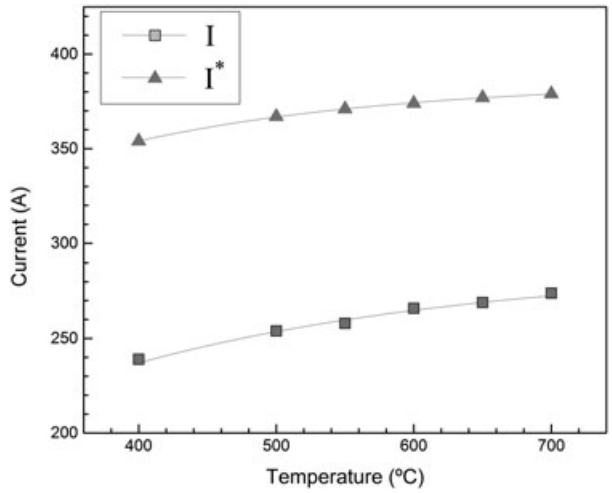

FIGURE A1 Steady measured and modelled electrical currents according to the control temperature

The origin of this discrepancy in the values of the electrical current is discussed in the value of the surface conductance parameter and the skin effect during the flow of alternating current in conductive materials. The value of h parameter has little influence in the modelled electrical current result; for example, if h is reduced 2 orders of magnitude, I^* drops 5 A at $T_c = 700°C$. Even more, the heat loss by radiation from the surface of the specimen can be neglected in the modelling of the heating by electric current in this kind of specimen. Skin effect is the tendency for AC current to flow mostly near the outer surface of an electrical conductor;[40] this implies a decrease of the section area of the specimen where the Joule effect occurs (the term $I^2\rho/A$ of Equation A1). If so, the heat source will have the same strength with less electrical current as seen by comparing our experimental data with the theoretical results. The decrease of the section area of the specimen can be taken in account through the concept of the skin depth (δ) defined as the distance at which the electrical current decreases to 1/e of its value at the conductor surface. The skin depth formula is given by

$$\delta = \sqrt{2\rho/\omega\mu_0\mu_r} \tag{A2}$$

where ω is the angular frequency of the current, μ_0 is the permeability of free space, and μ_r is the relative magnetic permeability of the conductor. Given these assumptions, the term describing the heat source in Equation A1 is corrected as follows,

$$\frac{I^2\rho}{A\text{effective}} = \frac{I^2\rho}{(2(a+b)\delta - 4\delta^2} \tag{A3}$$

where a and b are the height and the width of the specimen, respectively. The temperature dependence of the relative magnetic permeability considered for a reassessment of the electrical current by numerical calculation was obtained from Morishita et al41 for cold rolled carbon steel. After this correction, the agreement between measured and calculated currents was recovered.